

# QCS-SGM+: Improved Quantized Compressed Sensing with Score-Based Generative Models

Xiangming Meng<sup>1\*</sup>, Yoshiyuki Kabashima<sup>2</sup>

<sup>1</sup>The Zhejiang University-University of Illinois Urbana-Champaign Institute, Zhejiang University, China

<sup>2</sup>Institute for Physics of Intelligence & Department of Physics, The University of Tokyo, Japan  
xiangmingmeng@intl.zju.edu.cn, kaba@phys.s.u-tokyo.ac.jp

## Abstract

In practical compressed sensing (CS), the obtained measurements typically necessitate quantization to a limited number of bits prior to transmission or storage. This nonlinear quantization process poses significant recovery challenges, particularly with extreme coarse quantization such as 1-bit. Recently, an efficient algorithm called QCS-SGM was proposed for quantized CS (QCS) which utilizes score-based generative models (SGM) as an implicit prior. Due to the adeptness of SGM in capturing the intricate structures of natural signals, QCS-SGM substantially outperforms previous QCS methods. However, QCS-SGM is constrained to (approximately) row-orthogonal sensing matrices as the computation of the likelihood score becomes intractable otherwise. To address this limitation, we introduce an advanced variant of QCS-SGM, termed QCS-SGM+, capable of handling general matrices effectively. The key idea is a Bayesian inference perspective on the likelihood score computation, wherein expectation propagation is employed for its approximate computation. Extensive experiments are conducted, demonstrating the substantial superiority of QCS-SGM+ over QCS-SGM for general sensing matrices beyond mere row-orthogonality.

## 1 Introduction

Compressed sensing (CS) has emerged as a ubiquitous paradigm in signal processing and machine learning, aiming to accurately reconstruct high-dimensional signals from a limited number of measurements (Donoho 2006; Candès and Wakin 2008). The success of CS hinges on the assumption that, while the target signal may be high-dimensional, it possesses an inherent low-dimensional representation such as sparsity or low-rankness. Conventional CS models typically assume direct access to analog (continuous) measurements with infinite precision. In practice, however, analog measurements must be quantized into a finite number of digital bits using an analog-to-digital converter (ADC or quantizer) before further transmission, storage, or processing can occur (Boufounos and Baraniuk 2008; Zymnis, Boyd, and Candes 2009; Dai and Milenkovic 2011). In the extreme case, measurements are quantized into a single bit, retaining only the sign information while disregard-

ing the magnitude (Boufounos and Baraniuk 2008). Interestingly, 1-bit CS have gained attention due to their simplicity in hardware implementation and robustness against multiplicative errors (Boufounos and Baraniuk 2008; Zymnis, Boyd, and Candes 2009). Nevertheless, such nonlinear quantization operation invariably leads to information loss, thereby undermining the effectiveness of standard CS algorithms designed for analog measurements. To address this issue, a plethora of quantized CS (QCS) algorithms have been developed by explicitly considering the quantization effect (Boufounos and Baraniuk 2008; Zymnis, Boyd, and Candes 2009; Dai and Milenkovic 2011; Plan and Vershynin 2012, 2013; Jacques et al. 2013; Xu and Kabashima 2013; Xu, Kabashima, and Zdeborová 2014; Awasthi et al. 2016; Meng, Wu, and Zhu 2018; Jung et al. 2021; Liu et al. 2020; Liu and Liu 2022; Zhu et al. 2022; Meng and Kabashima 2023). Among these, the recently proposed algorithm QCS-SGM (Meng and Kabashima 2023) demonstrates exceptional state-of-the-art (SOTA) reconstruction performance under low-precision quantization levels. The key idea of QCS-SGM lies in utilizing the powerful score-based generative models (SGM, also known as diffusion models) (Song and Ermon 2019, 2020; Sohl-Dickstein et al. 2015; Ho, Jain, and Abbeel 2020; Nichol and Dhariwal 2021) as an implicit prior for the target signal. Intuitively, from a Bayesian perspective, the more accurate the prior obtained, the fewer observations required. Owing to SGM’s ability to capture the intricate structure of the target signal  $\mathbf{x}$  beyond simple sparsity, QCS-SGM can accurately reconstruct  $\mathbf{x}$  even from a small number of severely quantized noisy measurements.

While QCS-SGM exhibits remarkable performance, it has one fundamental limitation: it is derived under the assumption that the sensing matrix  $\mathbf{A}$  is (approximately) row-orthogonal. For general matrices, QCS-SGM’s performance will deteriorate since its computation of the *likelihood score* (defined in (4)) becomes less accurate (Meng and Kabashima 2023), as illustrated in Section 4.4. Although row-orthogonal matrices are prevalent in conventional CS, in practical applications one might encounter other types of matrices due to non-ideal physical constraints or design choices. In fact, the investigation of general sensing matrices has long been an active and important topic, such as the popular ill-conditioned matrices and correlated matrices, among others (Manoel et al. 2015; Schniter, Rangan,

\*Corresponding author.

and Fletcher 2016; Tanaka 2018; Ihara et al. 2018; Rangan, Schniter, and Fletcher 2019; Venkataramanan, Kögler, and Mondelli 2022; Zhu et al. 2022; Fan 2022). Despite these advances, much of existing work concentrates on standard CS or QCS with handcrafted sparsity. The study of QCS using SGM (diffusion models) for general sensing matrices, however, still remains a largely untouched research area. This paper try to address this problem and the main contributions are summarized as follows:

- We propose an advanced variant of QCS-SGM, designated as QCS-SGM+, which addresses the inherent limitation of the original QCS-SGM. Specifically, by treating the likelihood score computation as a Bayesian inference problem, QCS-SGM+ utilizes the well-established expectation propagation (EP) algorithm (Minka 2001) to yield a more refined approximation of the otherwise intractable likelihood score for general matrices.
- We validate the effectiveness of the proposed QCS-SGM+ in various experimental settings, encompassing diverse real-world datasets, distinct general matrices, and different noise levels. In each scenario, QCS-SGM+ consistently demonstrates remarkably superior performance over existing methods.

## 2 Related Work

Quantized compressed sensing (QCS) was first introduced in Boufounos and Baraniuk (2008); Zymnis, Boyd, and Candes (2009), after which it has become an important research topic and various QCS algorithms have been proposed, including some theoretical analysis (Dai and Milenkovic 2011; Plan and Vershynin 2012, 2013; Jacques et al. 2013; Xu and Kabashima 2013; Xu, Kabashima, and Zdeborová 2014; Awasthi et al. 2016; Meng, Wu, and Zhu 2018; Jung et al. 2021; Liu et al. 2020; Liu and Liu 2022; Zhu et al. 2022). With the recent advent of deep generative models (Goodfellow et al. 2014; Kingma and Welling 2013; Rezende and Mohamed 2015; Song and Ermon 2019, 2020; Sohl-Dickstein et al. 2015; Ho, Jain, and Abbeel 2020; Nichol and Dhariwal 2021), there has been a rising interest in CS methods with data-driven priors (Bora et al. 2017; Hand and Joshi 2019; Asim et al. 2020; Pan et al. 2021; Meng and Kabashima 2022). Specifically, following the pioneering CSGM framework (Bora et al. 2017), the prior  $p(\mathbf{x})$  of  $\mathbf{x}$  is learned through a generative model, such as VAE (Kingma and Welling 2013), GAN (Goodfellow et al. 2014), and score-based generative models (SGM) or diffusion models (DM) (Song and Ermon 2019, 2020; Sohl-Dickstein et al. 2015; Ho, Jain, and Abbeel 2020; Nichol and Dhariwal 2021). In the case of QCS, Liu et al. (2020); Liu and Liu (2022) extended the CSGM framework to non-linear observations such as 1-bit CS using VAE and GAN (in particular DCGAN (Radford, Metz, and Chintala 2015)). Surprisingly, SGM or DM (Song and Ermon 2019, 2020; Ho, Jain, and Abbeel 2020; Nichol and Dhariwal 2021) have demonstrated superior effectiveness, even surpassing state-of-the-art GAN (Goodfellow et al. 2014) and VAE (Kingma and Welling 2013) in generating diverse natural sources. In line with this, Meng and Kabashima (2023) recently pro-

posed a novel algorithm, QCS-SGM, employing SGM as an implicit prior, achieving state-of-the-art reconstruction performances for QCS. However, its application remains confined to (approximate) row-orthogonal sensing matrices.

## 3 Preliminary

### 3.1 System Model

The problem of quantized CS (QCS) can be mathematically formulated as follows (Boufounos and Baraniuk 2008; Zymnis, Boyd, and Candes 2009)

$$\mathbf{y} = \mathbf{Q}(\mathbf{A}\mathbf{x} + \mathbf{n}), \quad (1)$$

where the goal is to recover an unknown high-dimensional signal  $\mathbf{x} \in \mathbb{R}^{N \times 1}$  from a set of quantized measurements  $\mathbf{y} \in \mathbb{R}^{M \times 1}$ , where  $\mathbf{A} \in \mathbb{R}^{M \times N}$  is a known linear sensing matrix,  $\mathbf{n} \sim \mathcal{N}(\mathbf{n}; 0, \sigma^2 \mathbf{I})$  is an i.i.d. additive Gaussian noise, and  $\mathbf{Q}(\cdot) : \mathbb{R}^{M \times 1} \rightarrow \mathcal{Q}^{M \times 1}$  is an *element-wise* quantizer function which maps each element into a finite (or countable) set of codewords  $\mathcal{Q}$ , i.e.,  $y_m = \mathbf{Q}(z_m + n_m) \in \mathcal{Q}$ , or equivalently  $(z_m + n_m) \in \mathbf{Q}^{-1}(y_m)$ ,  $m = 1, 2, \dots, M$ , where  $z_m$  is the  $m$ -th element of  $\mathbf{z} = \mathbf{A}\mathbf{x}$ . Same as Meng and Kabashima (2023), we consider the uniform quantizer with  $Q$  quantization bits (resolution). The quantization codewords  $\mathcal{Q} = \{q_r\}_{r=1}^{2^Q}$  consist of  $2^Q$  elements, each with a quantization interval  $\mathbf{Q}^{-1}(q_r) = [l_{q_r}, u_{q_r})$ , where  $l_{q_r}$  and  $u_{q_r}$  are the lower and upper quantization threshold associated with the codeword  $q_r$ . In the extreme 1-bit case, i.e.,  $Q = 1$ , only the signs are observed so that (1) reduces to

$$\mathbf{y} = \text{sign}(\mathbf{A}\mathbf{x} + \mathbf{n}), \quad (2)$$

which corresponds to the well-known 1-bit CS and the quantization codewords are  $\mathcal{Q} = \{-1, +1\}$ .

### 3.2 QCS-SGM: Quantized CS with SGM

Compared to standard CS without quantization, QCS is particularly more challenging due to two key factors: (1) quantization leads to information loss, especially with low quantization resolution; (2) the nonlinearity of quantization operations can cause standard CS algorithms to deteriorate when applied directly. Recently, inspired by the prowess of SCM (Song and Ermon 2019; Song et al. 2020) in density estimation, Meng and Kabashima (2023) proposed an efficient method called QCS-SGM for QCS which can accurately reconstruct the target signal from a small number of severely quantized noisy measurements. The basic idea of QCS-SGM is to perform posterior sampling from  $p(\mathbf{x} | \mathbf{y})$  by using a learned SGM as an implicit prior (Meng and Kabashima 2023). Specifically, by utilizing the annealed Langevin dynamics (ALD) (Song et al. 2020), the posterior samples can be iteratively obtained as follows

$$\mathbf{x}_t = \mathbf{x}_{t-1} + \alpha_t \nabla_{\mathbf{x}_{t-1}} \log p(\mathbf{x}_{t-1} | \mathbf{y}) + \sqrt{2\alpha_t} \mathbf{z}_t, \quad 1 \leq t \leq T, \quad (3)$$

where the conditional (*posterior*) score  $\nabla_{\mathbf{x}_t} \log p(\mathbf{x}_t | \mathbf{y})$  is required. Using the Bayesian rule, the  $\nabla_{\mathbf{x}_t} \log p(\mathbf{x}_t | \mathbf{y})$  is decomposed into two terms

$$\underbrace{\nabla_{\mathbf{x}_t} \log p(\mathbf{x}_t | \mathbf{y})}_{\text{posterior score}} = \underbrace{\nabla_{\mathbf{x}_t} \log p(\mathbf{x}_t)}_{\text{prior score}} + \underbrace{\nabla_{\mathbf{x}_t} \log p(\mathbf{y} | \mathbf{x}_t)}_{\text{likelihood score}}, \quad (4)$$

including the unconditional score  $\nabla_{\mathbf{x}_t} \log p(\mathbf{x}_t)$  (called *prior score* in Meng and Kabashima (2023)), and the conditional score  $\nabla_{\mathbf{x}_t} \log p(\mathbf{y} | \mathbf{x}_t)$  (called *likelihood score* in Meng and Kabashima (2023)). While the prior score  $\nabla_{\mathbf{x}_t} \log p(\mathbf{x}_t)$  can be readily computed using a pre-trained score network, the likelihood score  $\nabla_{\mathbf{x}_t} \log p(\mathbf{y} | \mathbf{x}_t)$  is generally intractable. To circumvent this difficulty, Meng and Kabashima (2023) proposed a simple yet effective approximation of  $\nabla_{\mathbf{x}_t} \log p(\mathbf{y} | \mathbf{x}_t)$  under an uninformative prior assumption, whereby  $\mathbf{x}_t$  is approximated as  $\mathbf{x}_t = \mathbf{x} + \beta_t \tilde{\mathbf{n}}$ , where  $\tilde{\mathbf{n}} \sim \mathcal{N}(\mathbf{0}, \mathbf{I})$ . As a result, substituting it into (1), we obtain an equivalent representation as

$$\mathbf{y} = \mathbf{Q}(\mathbf{A}\mathbf{x}_t + \tilde{\mathbf{n}}_t), \quad (5)$$

where  $\tilde{\mathbf{n}}_t \sim \mathcal{N}(\mathbf{0}, \sigma^2 \mathbf{I} + \beta_t^2 \mathbf{A}\mathbf{A}^T)$  and  $\{\beta_t\}_{t=1}^T$  are a sequence of noise scales satisfying  $\beta_{\max} = \beta_1 > \beta_2 > \dots > \beta_T = \beta_{\min} > 0$  (Song et al. 2020). From (5), an approximation  $\tilde{p}(\mathbf{y} | \mathbf{z}_t = \mathbf{A}\mathbf{x}_t)$  (called *pseudo-likelihood*) of  $p(\mathbf{y} | \mathbf{x}_t)$  can be obtained as (Meng and Kabashima 2023)

$$\begin{aligned} p(\mathbf{y} | \mathbf{x}_t) &\simeq \tilde{p}(\mathbf{y} | \mathbf{z}_t = \mathbf{A}\mathbf{x}_t) \\ &= \int \prod_{m=1}^M 1((z_{t,m} + \tilde{n}_{t,m}) \in \mathbf{Q}^{-1}(y_m)) \mathcal{N}(\tilde{\mathbf{n}}_t; \mathbf{0}, \mathbf{C}_t^{-1}) d\tilde{\mathbf{n}}_t, \end{aligned} \quad (6)$$

where  $\mathbf{C}_t^{-1} = \sigma^2 \mathbf{I} + \beta_t^2 \mathbf{A}\mathbf{A}^T$  and  $z_{t,m}, \tilde{n}_{t,m}$  as the  $m$ -th elements of  $\mathbf{z}_t, \tilde{\mathbf{n}}_t$ , respectively, and  $1(\cdot)$  denotes the indicator function, i.e., it equals 1 if the event in the argument is true and equals 0 otherwise. Furthermore, under the assumption that  $\mathbf{A}$  is a row-orthogonal matrix such that  $\mathbf{A}\mathbf{A}^T$  (and thus the covariance matrix  $\mathbf{C}_t^{-1}$ ) becomes diagonal, Meng and Kabashima (2023) obtained a closed-form solution of the *pseudo-likelihood score*  $\nabla_{\mathbf{x}_t} \log \tilde{p}(\mathbf{y} | \mathbf{z}_t = \mathbf{A}\mathbf{x}_t)$ , which leads to QCS-SGM. Unfortunately, there is no closed-form solution for general matrices  $\mathbf{A}$ , which is the fundamental limitation of QCS-SGM. For more details of QCS-SGM and SGM, please refer to Meng and Kabashima (2023) and Song and Ermon (2019); Song et al. (2020), respectively.

## 4 Method

In this section, to address the inherent limitation of QCS-SGM (Meng and Kabashima 2023), we propose an enhanced variant, termed as QCS-SGM+, for general sensing matrices  $\mathbf{A}$ .

### 4.1 A New Perspective

Our key insight is that, the pseudo-likelihood term  $\tilde{p}(\mathbf{y} | \mathbf{z}_t = \mathbf{A}\mathbf{x}_t)$  (6) concerning  $\mathbf{x}_t$  can be alternatively interpreted as the partition function (normalization factor) of a posterior distribution concerning  $\tilde{\mathbf{n}}_t$  (rather than  $\mathbf{x}_t$ ), i.e.,

$$p(\tilde{\mathbf{n}}_t | \mathbf{y}) = \frac{f_b(\tilde{\mathbf{n}}_t) \prod_{m=1}^M f_a(\tilde{n}_{t,m})}{\tilde{p}(\mathbf{y} | \mathbf{z}_t = \mathbf{A}\mathbf{x}_t)}, \quad (7)$$

where  $f_b(\tilde{\mathbf{n}}_t) \equiv \mathcal{N}(\tilde{\mathbf{n}}_t; \mathbf{0}, \mathbf{C}_t^{-1})$  acts as the prior distribution, and  $f_a(\tilde{n}_{t,m}) \equiv 1((z_{t,m} + \tilde{n}_{t,m}) \in \mathbf{Q}^{-1}(y_m))$  acts as the likelihood distribution. As computing the partition function is one fundamental problem in Bayesian inference and

various approximate methods have been studied, such a perspective on  $\tilde{p}(\mathbf{y} | \mathbf{z}_t = \mathbf{A}\mathbf{x}_t)$  (6) as partition function provides us with one solution using well-studied approximate Bayesian inference methods (Wainwright and Jordan 2008).

### 4.2 Pseudo-Likelihood Score via EP

Due to its efficacy and available theoretical guarantee for some general matrices (Oppor and Winther 2001, 2005; Takahashi and Kabashima 2020), we resort to the well-known expectation propagation (EP) (Minka 2001) (also known as moment matching (Oppor and Winther 2005)) to approximately compute the intractable partition function  $\tilde{p}(\mathbf{y} | \mathbf{z}_t = \mathbf{A}\mathbf{x}_t)$  in (7), i.e., the pseudo-likelihood  $\tilde{p}(\mathbf{y} | \mathbf{z}_t = \mathbf{A}\mathbf{x}_t)$  (6). As illustrated in Figure 1, the basic idea is to apply EP to derive an effective factorized approximation of  $f_b(\tilde{\mathbf{n}}_t) \equiv \mathcal{N}(\tilde{\mathbf{n}}_t; \mathbf{0}, \mathbf{C}_t^{-1})$ . After EP, the original coupled prior node  $f_b(\tilde{\mathbf{n}}_t)$  in Figure 1 (a) is decoupled into a series of fully-factorized prior nodes  $f_c(\tilde{n}_{t,m}), m = 1 \dots M$  in 1 (b). Hence, a closed-form solution for  $\tilde{p}(\mathbf{y} | \mathbf{z}_t = \mathbf{A}\mathbf{x}_t)$  (7) can be obtained, thereby enabling us to compute the pseudo-likelihood score  $\nabla_{\mathbf{x}_t} \log \tilde{p}(\mathbf{y} | \mathbf{z}_t = \mathbf{A}\mathbf{x}_t)$ .

The details of our derivation via EP are illustrated as follows. Essentially, it approximates the partition function  $\tilde{p}(\mathbf{y} | \mathbf{z}_t = \mathbf{A}\mathbf{x}_t)$  (7) in three different ways as follows <sup>1</sup>:

$$\begin{aligned} \tilde{p}(\mathbf{y} | \mathbf{z}_t = \mathbf{A}\mathbf{x}_t) &\approx \\ &\begin{cases} \int \prod_{m=1}^M f_a(\tilde{n}_{t,m}) \mathcal{N}(\tilde{n}_{t,m}; \frac{h_m^F}{\tau^F}, \frac{1}{\tau^F}) d\tilde{\mathbf{n}}_t & (a) \\ \int \prod_{m=1}^M \mathcal{N}(\tilde{n}_{t,m}; \frac{h_m^G}{\tau^G}, \frac{1}{\tau^G}) f_b(\tilde{\mathbf{n}}_t) d\tilde{\mathbf{n}}_t & (b) \\ \int \prod_{m=1}^M \mathcal{N}(\tilde{n}_{t,m}; \frac{h_m^G}{\tau^G}, \frac{1}{\tau^G}) \mathcal{N}(\tilde{n}_{t,m}; \frac{h_m^F}{\tau^F}, \frac{1}{\tau^F}) d\tilde{\mathbf{n}}_t & (c) \end{cases} \end{aligned} \quad (8)$$

Intuitively, (8-a) approximates the correlated multivariate Gaussian  $f_b(\tilde{\mathbf{n}}_t) \equiv \mathcal{N}(\tilde{\mathbf{n}}_t; \mathbf{0}, \mathbf{C}_t^{-1})$  with a product of independent Gaussians  $\prod_{m=1}^M \mathcal{N}(\tilde{n}_{t,m}; \frac{h_m^F}{\tau^F}, \frac{1}{\tau^F})$ , (8-b) approximates the non-Gaussian likelihood  $f_a(\tilde{n}_{t,m}) \equiv 1((z_{t,m} + \tilde{n}_{t,m}) \in \mathbf{Q}^{-1}(y_m))$  with  $\mathcal{N}(\tilde{n}_{t,m}; \frac{h_m^G}{\tau^G}, \frac{1}{\tau^G})$ , and (8-c) combines the two approximations together. In contrast to the original intractable partition function  $\tilde{p}(\mathbf{y} | \mathbf{z}_t = \mathbf{A}\mathbf{x}_t)$  (7), all the three approximations (8-a), (8-b), (8-c) become tractable, leading to three closed-form approximations to the posterior mean  $\mathbb{E}[\tilde{n}_{t,m}]$  and variance  $\mathbb{V}[\tilde{n}_{t,m}]$  of  $\tilde{n}_{t,m}$  w.r.t.  $p(\tilde{\mathbf{n}}_t | \mathbf{y})$  (7), which are denoted as  $(m_m^a, \chi^a), (m_m^b, \chi^b), (m_m^c, \chi^c)$  respectively, and can be computed as follows

$$\begin{aligned} m_m^a &= \frac{h_m^F}{\tau^F} - \frac{2 \exp\left(-\frac{\tilde{u}_{ym}^2}{2}\right) - 2 \exp\left(-\frac{\tilde{l}_{ym}^2}{2}\right)}{\sqrt{2\pi\tau^F} \left[\text{erfc}\left(-\frac{\tilde{u}_{ym}}{\sqrt{2}}\right) - \text{erfc}\left(-\frac{\tilde{l}_{ym}}{\sqrt{2}}\right)\right]}, \quad (9) \\ \chi^a &= \frac{1}{\tau^F} - \frac{1}{M} \sum_{m=1}^M \left[ \frac{2\tilde{u}_{ym} \exp\left(-\frac{\tilde{u}_{ym}^2}{2}\right) - 2\tilde{l}_{ym} \exp\left(-\frac{\tilde{l}_{ym}^2}{2}\right)}{\sqrt{2\pi\tau^F} \left[\text{erfc}\left(-\frac{\tilde{u}_{ym}}{\sqrt{2}}\right) - \text{erfc}\left(-\frac{\tilde{l}_{ym}}{\sqrt{2}}\right)\right]} \right. \\ &\quad \left. + (m_m^a - \frac{h_m^F}{\tau^F})^2 \right], \quad (10) \end{aligned}$$

<sup>1</sup>The results might differ in a scaling factor but it does not affect the score function.

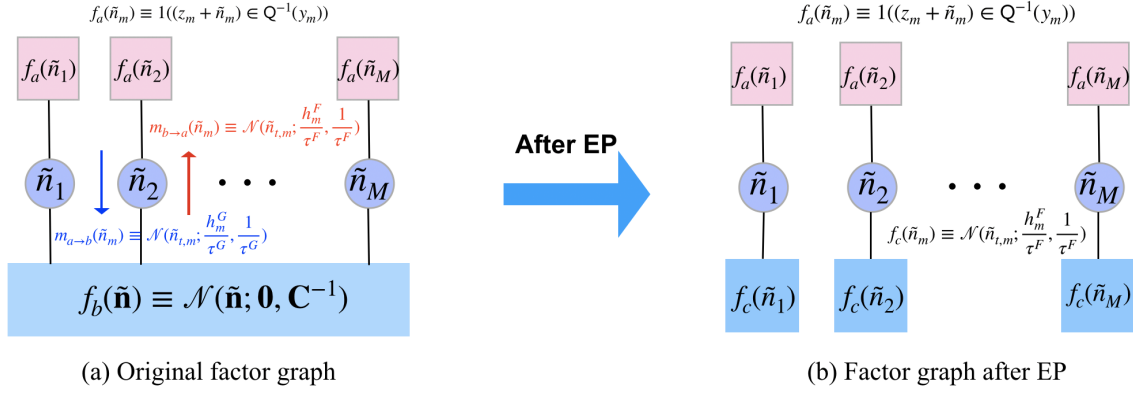


Figure 1: A schematic of the basic idea of QCS-SGM+ in computing the intractable pseudo-likelihood  $\tilde{p}(\mathbf{y}|\mathbf{z}_t = \mathbf{A}\mathbf{x}_t)$  for general matrices. The subscript  $t$  is dropped for simplicity. We resort to EP to obtain an effective factorized approximation of  $f_b(\tilde{\mathbf{n}})$  so that a closed-form solution of  $\tilde{p}(\mathbf{y}|\mathbf{z}_t = \mathbf{A}\mathbf{x}_t)$  can be achieved, which enables the computation of otherwise intractable pseudo-likelihood score.

$$m_m^b = [(\tau^G \mathbf{I} + \mathbf{C}_t)^{-1} \mathbf{h}^G]_m, \quad (11)$$

$$\chi^b = \text{Tr}[(\tau^G \mathbf{I} + \mathbf{C}_t)^{-1}] / M, \quad (12)$$

$$m_m^c = \frac{h_m^G + h_m^F}{\tau^G + \tau^F}, \quad (13)$$

$$\chi^c = \frac{1}{\tau^G + \tau^F}, \quad (14)$$

where  $\text{erfc}(z) = \frac{2}{\sqrt{\pi}} \int_z^\infty e^{-t^2} dt$  is the complementary error function (erfc) of the standard normal distribution,  $\text{Tr}[\cdot]$  is the trace of a matrix, and  $[\cdot]_m$  is the  $m$ -th element of a vector. In the special case of 1-bit quantization, i.e., sign measurements as described in (2), the results of  $(m_m^a, \chi^a)$  in (9, 10) and  $g_m$  in (24) can be further simplified as follows

$$m_m^a = \frac{h_m^F}{\tau^F} + \frac{2y_m e^{-\frac{\tilde{l}^2}{2}}}{\sqrt{2\pi\tau^F} \text{erfc}(\frac{y_m \tilde{l}}{\sqrt{2}})}, \quad (15)$$

$$\chi^a = \frac{1}{\tau^F} - \frac{1}{M} \sum_{m=1}^M \left[ (m_m^a - \frac{h_m^F}{\tau^F})^2 - \frac{2y_m \tilde{l} e^{-\frac{\tilde{l}^2}{2}}}{\sqrt{2\pi\tau^F} \text{erfc}(\frac{y_m \tilde{l}}{\sqrt{2}})} \right], \quad (16)$$

$$g_m = \frac{y_m \sqrt{2\tau^F} e^{-\frac{\tilde{l}^2}{2}}}{\sqrt{\pi} \text{erfc}(\frac{y_m \tilde{l}}{\sqrt{2}})}, \quad (17)$$

where  $\tilde{l} = -\sqrt{\tau^F} z_{t,m} - \frac{h_m^F}{\sqrt{\tau^F}}$ .

Subsequently, to determine the associated parameters  $(\mathbf{h}^F, \tau^F, \mathbf{h}^G, \tau^G)$  in (8), we leverage the moment matching condition of EP (Minka 2001; Oppor and Winther 2005), leading to the consistency of the associated posterior mean  $\mathbb{E}[\tilde{n}_{t,m}]$  and variance  $\mathbb{V}[\tilde{n}_{t,m}]$  of  $\tilde{n}_{t,m}$  from all the three approximations in (8), i.e.,

$$m_m^a = m_m^b = m_m^c, \quad (18)$$

$$\chi^a = \chi^b = \chi^c, \quad (19)$$

by which one can easily obtain  $(\mathbf{h}^F, \tau^F, \mathbf{h}^G, \tau^G)$  iteratively.

Interestingly, the above implementation details of EP can be illustrated via iterative message passing in the corresponding factor graphs (Minka 2001; Wainwright and Jordan 2008). As shown in Figure 1,  $\mathcal{N}(\tilde{n}_{t,m}; \frac{h_m^F}{\tau^F}, \frac{1}{\tau^F})$  corresponds to the message  $m_{b \rightarrow a}(\tilde{n}_m)$  from factor node  $f_b$  to factor node  $f_a$ , while  $\mathcal{N}(\tilde{n}_{t,m}; \frac{h_m^G}{\tau^G}, \frac{1}{\tau^G})$  corresponds to the message  $m_{a \rightarrow b}(\tilde{n}_m)$  from factor node  $f_a$  to factor node  $f_b$ . The three approximations (8-a), (8-b), and (8-c) correspond to the combined results of incoming messages in EP at factor node  $f_a$ , variable node  $\tilde{n}_m$ , factor node  $f_b$ , respectively.

After EP, as shown in Figure 1 (b), we can obtain an alternative factorized representation, leading to a closed-form approximation of  $\tilde{p}(\mathbf{y}|\mathbf{z}_t = \mathbf{A}\mathbf{x}_t)$  as follows

$$\tilde{p}(\mathbf{y}|\mathbf{z}_t = \mathbf{A}\mathbf{x}_t) \approx \frac{e^{\frac{(\mathbf{h}^F)^2}{2\tau^F}}}{2} \left[ \text{erfc}\left(\frac{-\tilde{u}_{y_m}}{\sqrt{2}}\right) - \text{erfc}\left(\frac{-\tilde{l}_{y_m}}{\sqrt{2}}\right) \right], \quad (20)$$

where

$$\tilde{u}_{y_m} = -\sqrt{\tau^F} z_{t,m} - \frac{h_m^F}{\sqrt{\tau^F}} + u_{y_m} \sqrt{\tau^F}, \quad (21)$$

$$\tilde{l}_{y_m} = -\sqrt{\tau^F} z_{t,m} - \frac{h_m^F}{\sqrt{\tau^F}} + l_{y_m} \sqrt{\tau^F}. \quad (22)$$

Therefore, from (6) and (20), the intractable pseudo-likelihood score  $\nabla_{\mathbf{x}_t} \log p(\mathbf{y} | \mathbf{x}_t)$  under quantized measurements  $\mathbf{y}$  in (1) can be approximated as

$$\nabla_{\mathbf{x}_t} \log p(\mathbf{y} | \mathbf{x}_t) \simeq \mathbf{A}^T \mathbf{G}(\beta_t, \mathbf{y}, \mathbf{A}, \mathbf{z}_t, \mathbf{h}^F, \tau^F), \quad (23)$$

where  $\mathbf{G}(\beta_t, \mathbf{y}, \mathbf{A}, \mathbf{z}_t, \mathbf{h}^F, \tau^F) = [g_1, g_2, \dots, g_M]^T \in \mathbb{R}^{M \times 1}$  with the  $m$ -th element being

$$g_m = -\frac{\sqrt{2\tau^F} \left[ \exp\left(-\frac{\tilde{u}_{y_m}^2}{2}\right) - \exp\left(-\frac{\tilde{l}_{y_m}^2}{2}\right) \right]}{\sqrt{\pi} \left[ \text{erfc}\left(-\frac{\tilde{u}_{y_m}}{\sqrt{2}}\right) - \text{erfc}\left(-\frac{\tilde{l}_{y_m}}{\sqrt{2}}\right) \right]}. \quad (24)$$

### 4.3 Resultant Algorithm: QCS-SGM+

By combining the pseudo-likelihood score (23) approximated via EP and the prior score from SGM, we readily obtain an enhanced version of QCS-SGM, dubbed as



QCS-SGM+, using the annealed Langevin dynamics (ALD) (Song and Ermon 2019). The details of QCS-SGM+ are shown in Algorithm 1 where the number of iterations of EP is denoted as *IterEP*. A scaling factor  $\gamma$  is introduced in QCS-SGM+, which is empirically found helpful to further improve the performance.

---

**Algorithm 1: QCS-SGM+**

---

**Input:**  $\{\beta_t\}_{t=1}^T, \epsilon, \gamma, \text{IterEP}, K, \mathbf{y}, \mathbf{A}, \sigma^2$ ,  
quantization thresholds  $\{[l_q, u_q) | q \in \mathcal{Q}\}$   
**Initialization:**  $\mathbf{x}_1^0 \sim \mathcal{U}(0, 1)$

```

1 for  $t = 1$  to  $T$  do
2    $\alpha_t \leftarrow \epsilon \beta_t^2 / \beta_T^2$ 
3   for  $k = 1$  to  $K$  do
4     Draw  $\mathbf{z}_t^k \sim \mathcal{N}(\mathbf{0}, \mathbf{I})$ 
5     Initialization:  $\mathbf{h}^F, \tau^F, \mathbf{h}^G, \tau^G$ 
6     for  $it = 1$  to  $\text{IterEP}$  do
7        $\mathbf{h}^G = \frac{\mathbf{m}^a}{\chi^a} - \mathbf{h}^F$ 
8        $\tau^G = \frac{1}{\chi^a} - \tau^F$ 
9        $\mathbf{h}^F = \frac{\mathbf{m}^b}{\chi^b} - \mathbf{h}^G$ 
10       $\tau^F = \frac{1}{\chi^b} - \tau^G$ 
11      Compute  $\nabla_{\mathbf{x}_t} \log p(\mathbf{y} | \mathbf{x}_t)$  as (23)
12       $\mathbf{x}_t^k = \mathbf{x}_t^{k-1} + \alpha_t [\mathbf{s}_\theta(\mathbf{x}_t^{k-1}, \beta_t) + \gamma \nabla_{\mathbf{x}_t} \log p(\mathbf{y} | \mathbf{x}_t)] + \sqrt{2\alpha_t} \mathbf{z}_t^k$ 
13    $\mathbf{x}_{t+1}^0 \leftarrow \mathbf{x}_t^K$ 

```

**Output:**  $\hat{\mathbf{x}} = \mathbf{x}_T^K$

---

Note that while it seems from (11, 12) that matrix inversion  $(\tau^G \mathbf{I} + \mathbf{C}_t)^{-1}$  is needed in each iteration for every  $\mathbf{C}_t$ , this is actually not the case since there exists one efficient implementation method using singular value decomposition (SVD) similar to Rangan, Schniter, and Fletcher (2019); Meng and Kabashima (2022). Specifically, denote  $\mathbf{A} = \mathbf{U}\Sigma\mathbf{V}^T$  as the SVD of  $\mathbf{A}$  and  $\Sigma^2$  as the element-wise square of singular values, i.e., diagonal elements of  $\Sigma$ , then after some simple algebra, it can be shown that the terms  $\mathbf{m}^b, \chi^b$  involving a matrix inverse can be efficiently computed as follows

$$\mathbf{m}^b = \mathbf{U} \text{diag}\left(\frac{\sigma^2 + \beta_t^2 \Sigma^2}{\tau_G(\sigma^2 + \beta_t^2 \Sigma^2) + 1}\right) \mathbf{U}^T \mathbf{h}^G, \quad (25)$$

$$\chi^b = \left\langle \frac{\sigma^2 + \beta_t^2 \Sigma^2}{\tau_G(\sigma^2 + \beta_t^2 \Sigma^2) + 1} \right\rangle, \quad (26)$$

where  $\langle \cdot \rangle$  is the average value of the elements in a vector. It can be seen from (25, 26) that one simply needs to replace the values of  $\beta_t, \tau_G$  for different iterations. Hence, the main computational burden lies in the SVD of sensing matrix  $\mathbf{A}$ , but only one time is required in the whole QCS-SGM+.

#### 4.4 Relation to QCS-SGM

For row-orthogonal matrices  $\mathbf{A}$ , the covariance matrix  $\mathbf{C}_t^{-1} = \sigma^2 \mathbf{I} + \beta_t^2 \mathbf{A} \mathbf{A}^T$  becomes diagonal and thus the

prior node  $f_b(\tilde{\mathbf{n}}_t) \equiv \mathcal{N}(\tilde{\mathbf{n}}_t; \mathbf{0}, \mathbf{C}_t^{-1})$  in Figure 1 (a) already fully factorizes and thus QCS-SGM+ ( $\gamma = 1$ ) reduces to QCS-SGM (Meng and Kabashima 2023). For general matrices  $\mathbf{A}$ , however, there is no such equivalence even though QCS-SGM can still be applied pretending  $\mathbf{C}_t^{-1}$  to be diagonal, i.e., QCS-SGM directly diagonalizes  $\mathbf{C}_t^{-1}$  by extracting its main diagonal elements. The fundamental difference between QCS-SGM and QCS-SGM+ can be better illustrated from the new perspective on  $\tilde{p}(\mathbf{y} | \mathbf{z}_t = \mathbf{A} \mathbf{x}_t)$  as partition function  $\tilde{p}(\mathbf{y} | \mathbf{z}_t = \mathbf{A} \mathbf{x}_t) = \int f_b(\tilde{\mathbf{n}}_t) \prod_{m=1}^M f_a(\tilde{n}_{t,m}) d\mathbf{n}_t$  (7). QCS-SGM naively diagonalizes the correlated Gaussian  $f_b(\tilde{\mathbf{n}}_t) \equiv \mathcal{N}(\tilde{\mathbf{n}}_t; \mathbf{0}, \mathbf{C}_t^{-1})$ , which ignores the effect of  $\prod_{m=1}^M f_a(\tilde{n}_{t,m})$ ; by contrast, QCS-SGM+ considers  $f_b(\tilde{\mathbf{n}}_t) \prod_{m=1}^M f_a(\tilde{n}_{t,m})$  as a whole and diagonalizes  $f_b(\tilde{\mathbf{n}}_t)$  by explicitly takes into account the effect of  $\prod_{m=1}^M f_a(\tilde{n}_{t,m})$ , thereby leading to better performances than QCS-SGM for general matrices  $\mathbf{A}$ .

## 5 Experiments

We empirically demonstrate the efficacy of the proposed QCS-SGM+ in various scenarios. The source code is available at <https://github.com/mengxiangming/QCS-SGM-plus>. More results, including the detailed hyper-parameter setting, can be found in the appendix.

Specifically, we investigate two popular general sensing matrices  $\mathbf{A}$  beyond row-orthogonal:

(a) **ill-conditioned matrices** (Rangan, Schniter, and Fletcher 2019; Schniter, Rangan, and Fletcher 2016; Venkataramanan, Kögler, and Mondelli 2022; Fan 2022):  $\mathbf{A} = \mathbf{V}\Sigma\mathbf{U}^T$ , where  $\mathbf{V}$  and  $\mathbf{U}$  are independent Haar-distributed matrices, and the nonzero singular values of  $\mathbf{A}$  satisfy  $\frac{\lambda_i}{\lambda_{i+1}} = \kappa^{1/M}$ , where  $\kappa$  is the condition number. Such matrices can have an arbitrary spectral distribution and often arise in practical applications (Venkataramanan, Kögler, and Mondelli 2022).

(b) **correlated matrices** (Shiu et al. 2000; Zhu et al. 2022):  $\mathbf{A}$  is constructed as  $\mathbf{A} = \mathbf{R}_L \mathbf{H} \mathbf{R}_R$ , where  $\mathbf{R}_L = \mathbf{R}_1^{\frac{1}{2}} \in \mathbb{R}^{M \times M}$  and  $\mathbf{R}_R = \mathbf{R}_2^{\frac{1}{2}} \in \mathbb{R}^{N \times N}$ , the  $(i, j)$ th element of both  $\mathbf{R}_1$  and  $\mathbf{R}_2$  is  $\rho^{|i-j|}$  and  $\rho$  is termed as the correlation coefficient here,  $\mathbf{H} \in \mathbb{R}^{M \times N}$  is a random matrix whose elements are drawn i.i.d. from  $\mathcal{N}(0, 1)$ .

**Datasets:** We consider three popular datasets: MNIST (LeCun and Cortes 2010), CIFAR-10 (Krizhevsky and Hinton 2009), and CelebA (Liu et al. 2015). For CelebA dataset, we cropped each face image to a  $64 \times 64$  RGB image, resulting in  $N = 64 \times 64 \times 3 = 12288$  inputs per image.

**QCS-SGM+:** Same as QCS-SGM (Meng and Kabashima 2023), we adopt the NCSNv2 (Song and Ermon 2020) in all cases. For MNIST, the NCSNv2 was trained with a similar training set up as CIFAR-10 in Song and Ermon (2020), while for CIFAR-10, and CelebA, we use the pre-trained models from <https://drive.google.com/drive/folders/1217uhIvLg9ZrYnKOR3XTRFSurt4miQrd>.

**Comparison Methods:** We compare QCS-SGM+ with not only the state-of-the-art QCS-SGM (Meng and Kabashima 2023), but also two other leading methods before QCS-SGM, namely BIPG (Liu et al. 2020) and OneShot

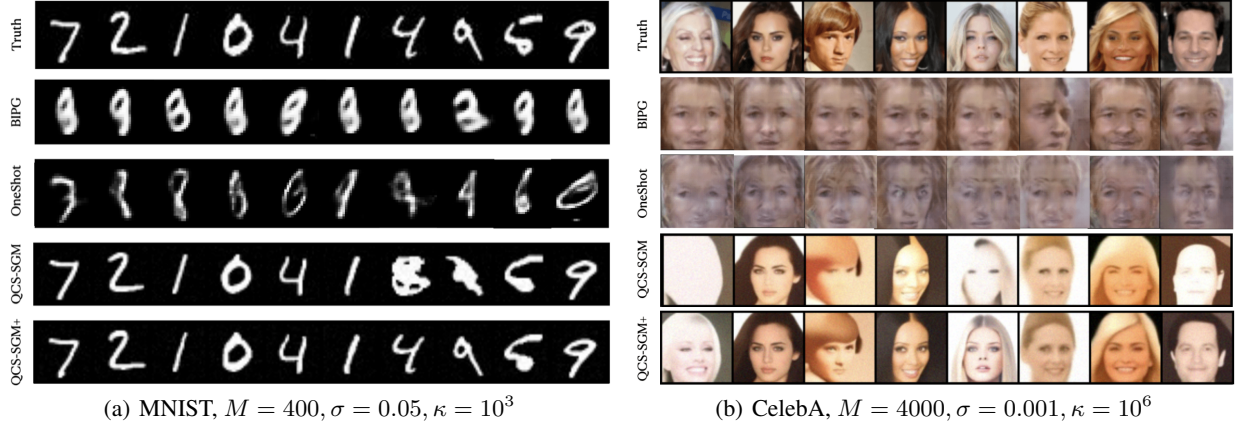


Figure 2: Qualitative comparisons of different methods under 1-bit CS on MNIST and CelebA for ill-conditioned  $\mathbf{A}$  ( $\kappa = 10^3$  for MNIST and  $\kappa = 10^6$  for CelebA) when  $M < N$ . It can be seen that QCS-SGM+ apparently outperforms the original QCS-SGM and other methods.

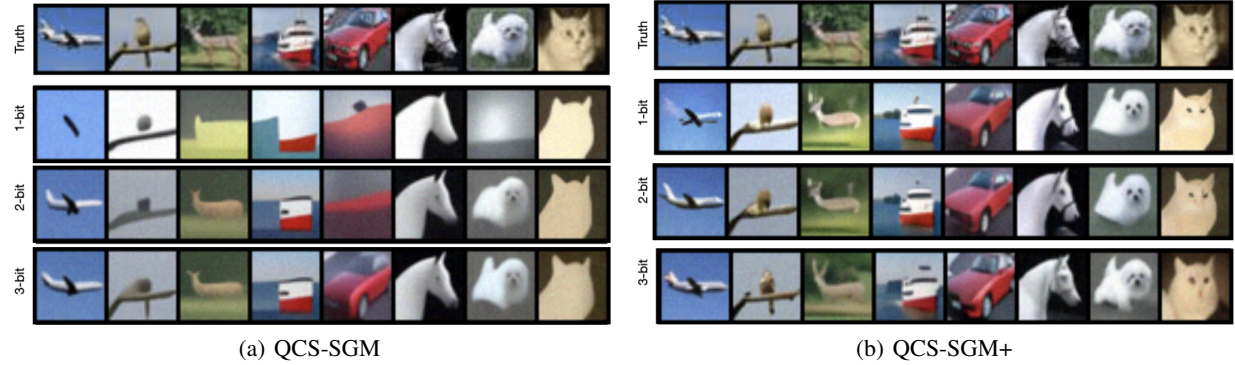


Figure 3: Reconstructed images on CIFAR-10 with QCS-SGM and QCS-SGM+, respectively, under 1-3 bit CS when the condition number of  $\mathbf{A}$  is 1000,  $M = 2000, \sigma = 0.1$ . QCS-SGM+ achieves significantly better results than QCS-SGM.

(Liu and Liu 2022).

## 5.1 Qualitative Results

Figure 2 shows some qualitative results of QCS-SGM+ and QCS-SGM, BIFG, and OneShot under 1-bit CS for ill-conditioned  $\mathbf{A}$ . It can be seen from Figure 2 that the proposed QCS-SGM+ achieves remarkably better performances than all previous methods and can well reconstructs the target images from only a few  $M < N$  sign measurements even when the sensing matrix  $\mathbf{A}$  is highly ill-conditioned. To further demonstrate the efficacy of QCS-SGM+ under different quantization resolutions (e.g., 1-3 bits), Figure 3 shows some results of QCS-SGM and QCS-SGM+, respectively, with condition number of  $\mathbf{A}$  being  $\kappa = 10^3$  and  $\sigma = 0.1$ . It can be seen that QCS-SGM+ is able to generate clear images even with  $M < N$  1-3 bit noisy quantized measurements, whereas the original QCS-SGM yields only vague or blurry results.

## 5.2 Quantitative Results

The quantitative comparison in terms of the peak signal-to-noise ratio (PSNR) is evaluated. First, Figure 4 illustrates

the PSNR results of QCS-SGM+ and QCS-SGM, in the case of 1-bit CS with MNIST, CIFAR-10, and CelebA, for ill-conditioned  $\mathbf{A}$  and correlated  $\mathbf{A}$ , respectively. It can be seen that in all cases, the proposed QCS-SGM+ achieves much better performances, demonstrating the superiority of QCS-SGM+ over QCS-SGM for more general sensing matrices  $\mathbf{A}$ . We also evaluate the effect of Gaussian noise  $\mathbf{n} \sim \mathcal{N}(\mathbf{n}; 0, \sigma^2 \mathbf{I})$  by conducting experiments on 1-bit CS with different levels of noise standard deviation (std)  $\sigma$ . As shown in Figure 5, due to the potential dithering effect, QCS-SGM+ with noise can sometimes achieve slightly better results than that without noise. Generally, QCS-SGM+ is robust to noise and can achieve good results in a large range of  $\mathbf{n}$ , while significantly outperforming QCS-SGM.

## 6 Conclusion

In this paper, we propose an improved version of QCS-SGM, termed as QCS-SGM+, for quantized compressed sensing under general sensing matrices. By viewing the likelihood computation as a Bayesian inference problem, QCS-SGM+ approximates the intractable likelihood score using the well-known EP. To verify the effectiveness of QCS-

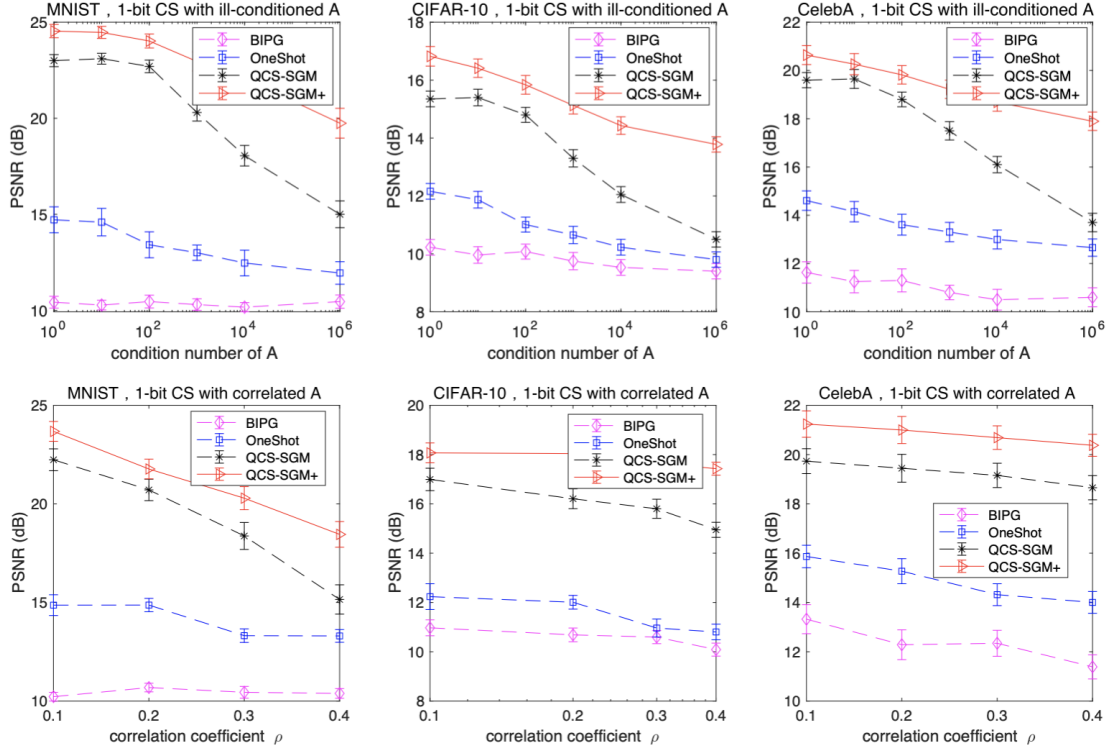


Figure 4: Quantitative comparisons between QCS-SGM+ and existing methods under 1-bit CS for MNIST, CIFAR-10, and CelebA when the sensing matrices  $\mathbf{A}$  are ill-conditioned and correlated, respectively. The number of measurements are  $M = 400, 2000, 4000$  for MNIST, CIFAR-10, and CelebA, respectively, all satisfying  $M < N$ . Standard error bars for the results are also shown.

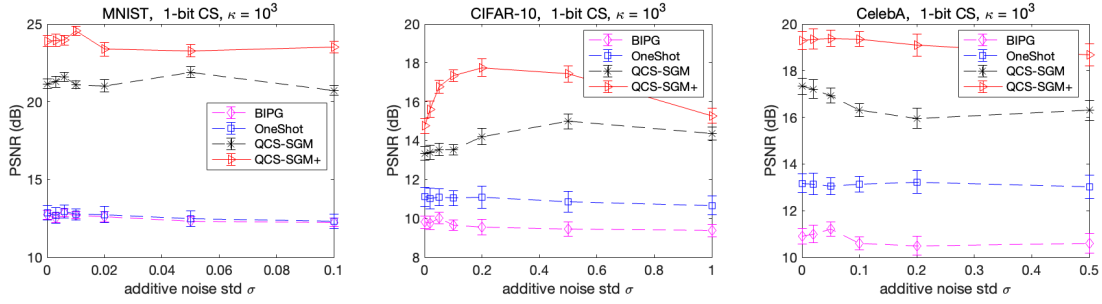


Figure 5: Quantitative comparisons between QCS-SGM+ and other methods under 1-bit CS with different levels of Gaussian noise for ill-conditioned  $\mathbf{A}$  with condition number  $\kappa = 10^3$ . The number of measurements are  $M = 400, 2000, 4000$  for MNIST, CIFAR-10, and CelebA, respectively, all satisfying  $M < N$ . Standard error bars for the results are also shown.

SGM+, we conducted experiments on a variety of baseline datasets, demonstrating that QCS-SGM+ significantly outperforms QCS-SGM by a large margin for general sensing matrices. There are several limitations of QCS-SGM+. For example, QCS-SGM+ requires EP message passing, which is computationally slower than QCS-SGM. Also, same as QCS-SGM, it requires a large number of iterations to generate one posterior sample. As future work, it is important to further reduce the complexity of QCS-SGM+ and develop more efficient alternatives with more advanced diffusion models. Moreover, a theoretical analysis of both QCS-SGM and QCS-SGM+ is also an important future direction.

## Acknowledgements

This work was supported by NSFC No. 62306277, and the NSFC Excellent Young Scholars Fund (Overseas), China, and JSPS KAKENHI Nos. 17H00764, 18K11463, and 19H01812, 22H05117, and JST CREST Grant Number JP-MJCR1912, Japan.

## References

Asim, M.; Daniels, M.; Leong, O.; Ahmed, A.; and Hand, P. 2020. Invertible generative models for inverse problems: mitigating representation error and dataset bias. In *International Conference on Machine Learning*, 399–409. PMLR.

- Awasthi, P.; Balcan, M.-F.; Haghtalab, N.; and Zhang, H. 2016. Learning and 1-bit compressed sensing under asymmetric noise. In *Conference on Learning Theory*, 152–192. PMLR.
- Bora, A.; Jalal, A.; Price, E.; and Dimakis, A. G. 2017. Compressed sensing using generative models. In *International Conference on Machine Learning*, 537–546. PMLR.
- Boufounos, P. T.; and Baraniuk, R. G. 2008. 1-Bit compressive sensing. In *2008 42nd Annual Conference on Information Sciences and Systems*, 16–21.
- Candès, E. J.; and Wakin, M. B. 2008. An introduction to compressive sampling. *IEEE signal processing magazine*, 25(2): 21–30.
- Dai, W.; and Milenkovic, O. 2011. Information theoretical and algorithmic approaches to quantized compressive sensing. *IEEE transactions on communications*, 59(7): 1857–1866.
- Donoho, D. L. 2006. Compressed sensing. *IEEE Transactions on information theory*, 52(4): 1289–1306.
- Fan, Z. 2022. Approximate message passing algorithms for rotationally invariant matrices. *The Annals of Statistics*, 50(1): 197–224.
- Goodfellow, I.; Pouget-Abadie, J.; Mirza, M.; Xu, B.; Warde-Farley, D.; Ozair, S.; Courville, A.; and Bengio, Y. 2014. Generative Adversarial Nets. In Ghahramani, Z.; Welling, M.; Cortes, C.; Lawrence, N.; and Weinberger, K., eds., *Advances in Neural Information Processing Systems*, volume 27. Curran Associates, Inc.
- Hand, P.; and Joshi, B. 2019. Global guarantees for blind demodulation with generative priors. *Advances in Neural Information Processing Systems*, 32.
- Ho, J.; Jain, A.; and Abbeel, P. 2020. Denoising diffusion probabilistic models. *Advances in Neural Information Processing Systems*, 33: 6840–6851.
- Ihara, M.; Iwata, K.; Suematsu, N.; and Mimura, K. 2018. Typical Performance of Sparse Signal Recovery from a Linear Measurement with Large Coherence. In *2018 International Symposium on Information Theory and Its Applications (ISITA)*, 427–431. IEEE.
- Jacques, L.; Laska, J. N.; Boufounos, P. T.; and Baraniuk, R. G. 2013. Robust 1-bit compressive sensing via binary stable embeddings of sparse vectors. *IEEE transactions on information theory*, 59(4): 2082–2102.
- Jalal, A.; Arvinte, M.; Daras, G.; Price, E.; Dimakis, A. G.; and Tamir, J. 2021. Robust compressed sensing mri with deep generative priors. *Advances in Neural Information Processing Systems*, 34: 14938–14954.
- Jung, H. C.; Maly, J.; Palzer, L.; and Stollenwerk, A. 2021. Quantized compressed sensing by rectified linear units. *IEEE transactions on information theory*, 67(6): 4125–4149.
- Kingma, D. P.; and Welling, M. 2013. Auto-encoding variational bayes. *arXiv preprint arXiv:1312.6114*.
- Krizhevsky, A.; and Hinton, G. 2009. Learning multiple layers of features from tiny images. Technical report, Citeseer.
- LeCun, Y.; and Cortes, C. 2010. MNIST handwritten digit database.
- Liu, J.; and Liu, Z. 2022. Non-Iterative Recovery from Non-linear Observations using Generative Models. In *Proceedings of the IEEE/CVF Conference on Computer Vision and Pattern Recognition*, 233–243.
- Liu, Z.; Gomes, S.; Tiwari, A.; and Scarlett, J. 2020. Sample complexity bounds for 1-bit compressive sensing and binary stable embeddings with generative priors. In *International Conference on Machine Learning*, 6216–6225. PMLR.
- Liu, Z.; Luo, P.; Wang, X.; and Tang, X. 2015. Deep Learning Face Attributes in the Wild. In *Proceedings of International Conference on Computer Vision (ICCV)*.
- Manoel, A.; Krzakala, F.; Tramel, E.; and Zdeborova, L. 2015. Swept approximate message passing for sparse estimation. In *International Conference on Machine Learning*, 1123–1132. PMLR.
- Meng, X.; and Kabashima, Y. 2022. Diffusion Model Based Posterior Sampling for Noisy Linear Inverse Problems. *arXiv preprint arXiv:2211.12343*.
- Meng, X.; and Kabashima, Y. 2023. Quantized Compressed Sensing with Score-Based Generative Models. In *International Conference on Learning Representations*.
- Meng, X.; Wu, S.; and Zhu, J. 2018. A unified Bayesian inference framework for generalized linear models. *IEEE Signal Processing Letters*, 25(3): 398–402.
- Minka, T. P. 2001. Expectation propagation for approximate Bayesian inference. In *Proceedings of the Seventeenth conference on Uncertainty in artificial intelligence*, 362–369.
- Nichol, A. Q.; and Dhariwal, P. 2021. Improved denoising diffusion probabilistic models. In *International Conference on Machine Learning*, 8162–8171. PMLR.
- Opper, M.; and Winther, O. 2001. Tractable approximations for probabilistic models: The adaptive Thouless-Anderson-Palmer mean field approach. *Physical Review Letters*, 86(17): 3695.
- Opper, M.; and Winther, O. 2005. Expectation Consistent Approximate Inference. *Journal of Machine Learning Research*, 6: 2177–2204.
- Pan, X.; Zhan, X.; Dai, B.; Lin, D.; Loy, C. C.; and Luo, P. 2021. Exploiting deep generative prior for versatile image restoration and manipulation. *IEEE Transactions on Pattern Analysis and Machine Intelligence*.
- Plan, Y.; and Vershynin, R. 2012. Robust 1-bit compressed sensing and sparse logistic regression: A convex programming approach. *IEEE Transactions on Information Theory*, 59(1): 482–494.
- Plan, Y.; and Vershynin, R. 2013. One-bit compressed sensing by linear programming. *Communications on Pure and Applied Mathematics*, 66(8): 1275–1297.
- Radford, A.; Metz, L.; and Chintala, S. 2015. Unsupervised representation learning with deep convolutional generative adversarial networks. *arXiv preprint arXiv:1511.06434*.
- Rangan, S.; Schniter, P.; and Fletcher, A. K. 2019. Vector approximate message passing. *IEEE Transactions on Information Theory*, 65(10): 6664–6684.

- Rezende, D.; and Mohamed, S. 2015. Variational inference with normalizing flows. In *International conference on machine learning*, 1530–1538. PMLR.
- Schniter, P.; Rangan, S.; and Fletcher, A. K. 2016. Vector approximate message passing for the generalized linear model. In *2016 50th Asilomar conference on signals, systems and computers*, 1525–1529. IEEE.
- Shiu, D.-S.; Foschini, G. J.; Gans, M. J.; and Kahn, J. M. 2000. Fading correlation and its effect on the capacity of multielement antenna systems. *IEEE Transactions on communications*, 48(3): 502–513.
- Sohl-Dickstein, J.; Weiss, E.; Maheswaranathan, N.; and Ganguli, S. 2015. Deep unsupervised learning using nonequilibrium thermodynamics. In *International Conference on Machine Learning*, 2256–2265. PMLR.
- Song, Y.; and Ermon, S. 2019. Generative modeling by estimating gradients of the data distribution. *Advances in Neural Information Processing Systems*, 32.
- Song, Y.; and Ermon, S. 2020. Improved techniques for training score-based generative models. *Advances in neural information processing systems*, 33: 12438–12448.
- Song, Y.; Sohl-Dickstein, J.; Kingma, D. P.; Kumar, A.; Ermon, S.; and Poole, B. 2020. Score-Based Generative Modeling through Stochastic Differential Equations. In *International Conference on Learning Representations*.
- Takahashi, T.; and Kabashima, Y. 2020. Semi-analytic approximate stability selection for correlated data in generalized linear models. *Journal of Statistical Mechanics: Theory and Experiment*, 2020(9): 093402.
- Tanaka, T. 2018. Performance analysis of L 1-norm minimization for compressed sensing with non-zero-mean matrix elements. In *2018 IEEE International Symposium on Information Theory (ISIT)*, 401–405. IEEE.
- Venkataramanan, R.; Kögler, K.; and Mondelli, M. 2022. Estimation in rotationally invariant generalized linear models via approximate message passing. In *International Conference on Machine Learning*, 22120–22144. PMLR.
- Wainwright, M. J.; and Jordan, M. I. 2008. *Graphical models, exponential families, and variational inference*. Now Publishers Inc.
- Xu, Y.; and Kabashima, Y. 2013. Statistical mechanics approach to 1-bit compressed sensing. *Journal of Statistical Mechanics: Theory and Experiment*, 2013(02): P02041.
- Xu, Y.; Kabashima, Y.; and Zdeborová, L. 2014. Bayesian signal reconstruction for 1-bit compressed sensing. *Journal of Statistical Mechanics: Theory and Experiment*, 2014(11): P11015.
- Zhu, J.; Meng, X.; Lei, X.; and Guo, Q. 2022. A Unitary Transform Based Generalized Approximate Message Passing. *arXiv preprint arXiv:2210.08861*.
- Zymnis, A.; Boyd, S.; and Candes, E. 2009. Compressed sensing with quantized measurements. *IEEE Signal Processing Letters*, 17(2): 149–152.



## A Hyper-parameter Setting of QCS-SGM+

As shown in Algorithm 1, there are several hyper-parameters in the proposed QCS-SGM+, including  $\{\beta_t\}_{t=1}^T$ ,  $\epsilon$ ,  $\gamma$ ,  $IterEP$ ,  $K$ . Among them, the values of  $\{\beta_t\}_{t=1}^T$  and  $K$  are exactly the same as the pre-trained SGM model, i.e., once the pre-trained SGM model is given,  $\{\beta_t\}_{t=1}^T$  and  $K$  are fixed as the same value as the SGM. The step size  $\epsilon$  is set to be the same as QCS-SGM, which is a constant value (here, same as QCS-SGM, we set  $\epsilon$  to be  $\epsilon = 0.002$  in all the experiments), though some further improvement can be expected with a careful fine-tuning of it.

Regarding the scaling factor  $\gamma$  of QCS-SGM+, it is set as follows

$$\gamma = \xi \frac{\|\mathbf{s}_\theta(\mathbf{x}_t^{k-1}, \beta_t)\|}{\|\nabla_{\mathbf{x}_t} \log p_{\beta_t}(\mathbf{y} | \mathbf{x}_t)\|}, \quad (27)$$

where  $\xi > 0$  is another induced scalar hyper-parameter. In the original QCS-SGM, no  $\gamma$  is introduced, i.e., it is simply set to be a fixed value  $\gamma = 1$ . However, it is empirically found that adding a proper scaling factor  $\gamma$  leads to a better performance (as shown in Figure 6). The choice of the form in (27) is inspired from Jalal et al. (2021).

Regarding the number of iterations  $IterEP$  of QCS-SGM+, it is empirically found that 3-5 iterations are enough in most cases (as shown in Figure 6). As a result, if there is no further illustration, the experimental results shown in this paper are all using  $IterEP = 5$  by default.

To illustrate the effect of  $\gamma$  and  $IterEP$  of QCS-SGM+, Figure 6 shows 1-bit CS results of QCS-SGM+ on various datasets with (w.t.) and without (w.o.) scaling factor  $\gamma$  for different number of EP iterations  $IterEP$ . Specifically, we set  $\xi = 0.5$  for both MNIST and CIFAR-10, and  $\xi = 0.3$  for CelebA for QCS-SGM+ w.t.  $\gamma$  in all the related experiments. It can be seen that in both cases with and without  $\gamma$ , QCS-SGM+ converges with 3-5 EP iterations. Interestingly, when the sensing matrix  $\mathbf{A}$  deviates from row-orthogonal matrix, i.e., the condition number becomes much larger than 1, QCS-SGM+ w.o.  $\gamma$  apparently outperforms the original QCS-SGM, demonstrating the efficacy of EP in QCS-SGM+. Furthermore, QCS-SGM+ w.t.  $\gamma$  further improves QCS-SGM+ w.o.  $\gamma$  by introducing the scaling factor  $\gamma$ . Overall, the proposed QCS-SGM+ significantly outperforms the original QCS-SGM.

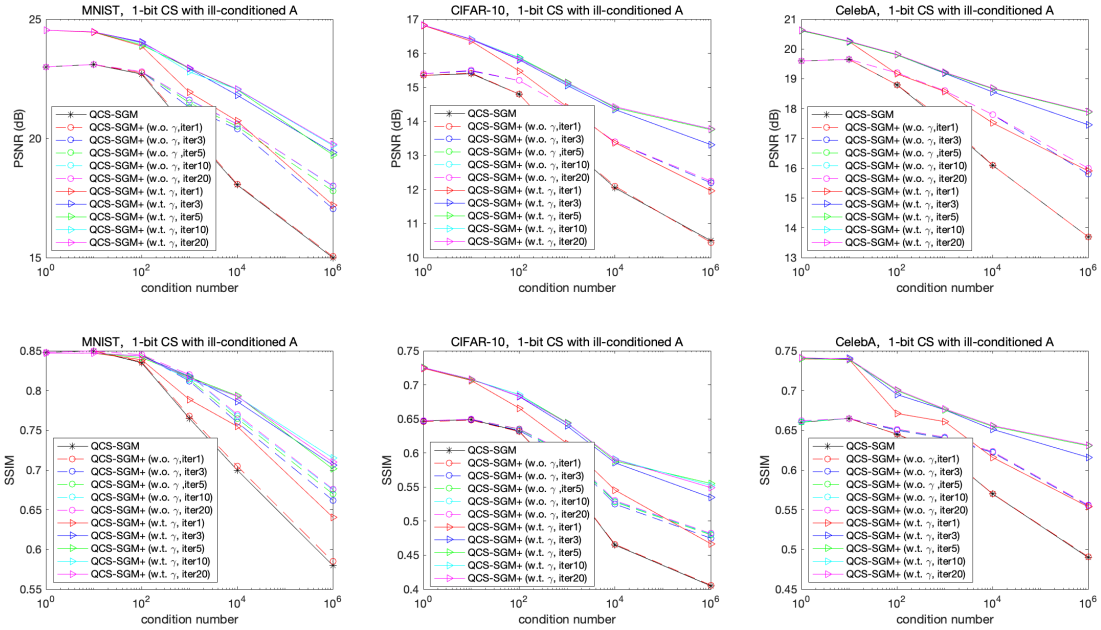


Figure 6: 1-bit CS results of QCS-SGM+ on various datasets with (w.t.) and without (w.o.) scaling factor  $\gamma$  for different number of EP iterations  $IterEP$ . In this example, the sensing matrix  $\mathbf{A}$  used is ill-conditioned with different condition numbers. Note that both PSNR and SSIM results are shown.

## B Additional Results

All the experiments are conducted on one NVIDIA Tesla V100. In this appendix, we show some additional results apart from those in the main text.

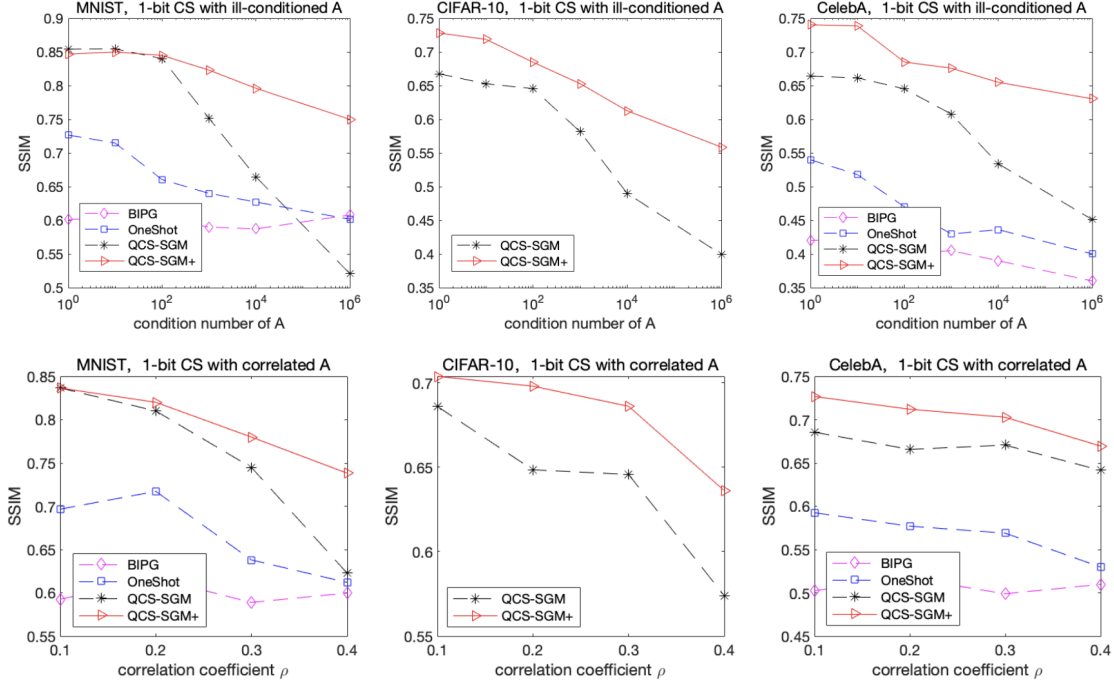


Figure 7: Quantitative comparisons (in terms of SSIM) of the proposed QCS-SGM+ and the original QCS-SGM under 1-bit CS for MNIST, CIFAR-10, and CelebA datasets when the measurement matrices  $\mathbf{A}$  are ill-conditioned and correlated, respectively. The number of measurements are set to be  $M = 400, 2000, 4000$  for MNIST, CIFAR-10, and CelebA, respectively, all satisfying  $M < N$ . In all cases, QCS-SGM+ apparently outperforms QCS-SGM.

## B.1 Quantitative Results in terms of SSIM

In this section, we provide additional quantitative results in terms of the structural similarity index measure (SSIM). As shown in Figure 7 and Figure 8, similar to the PSNR metric, the proposed QCS-SGM+ significantly outperforms QCS-SGM as well as BIPG and OneShot in terms of SSIM. Note that results of BIPG and OneShot for CIFAR-10 are not shown since there is a lack of pre-trained model in their open-sourced code.

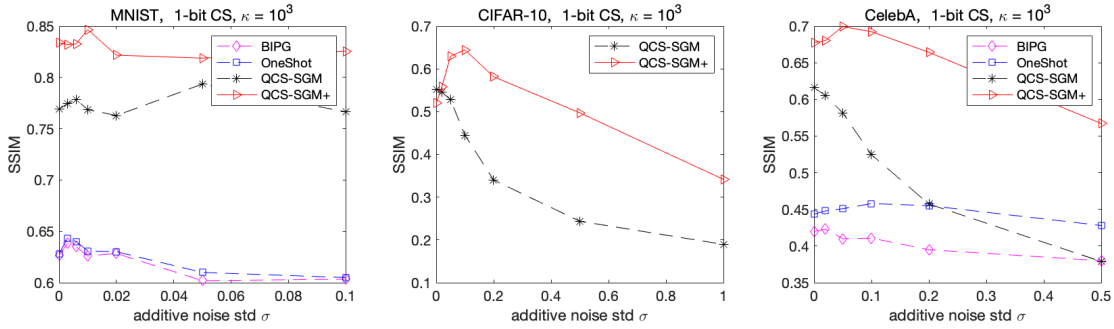
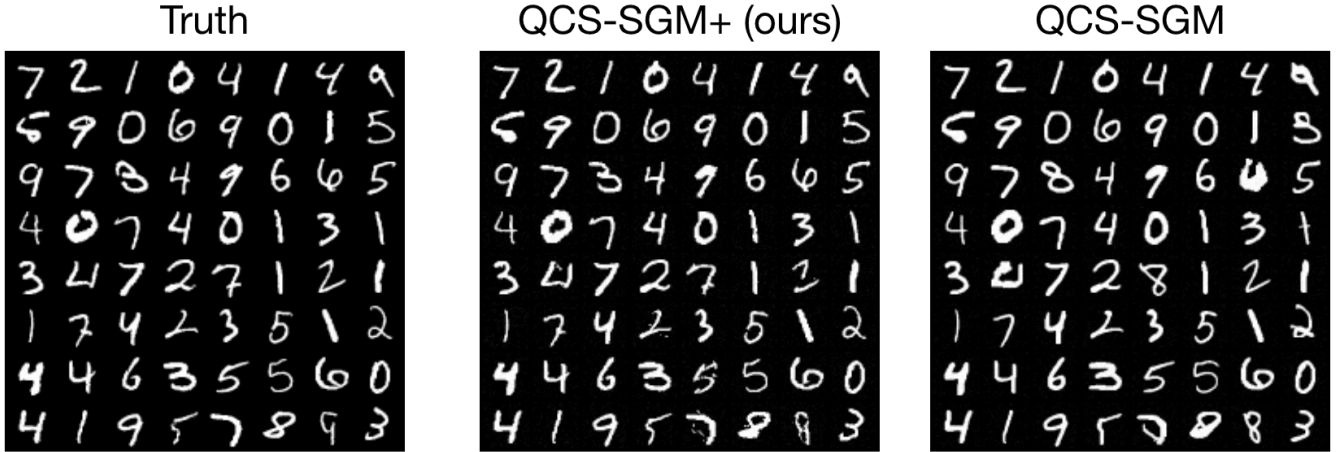


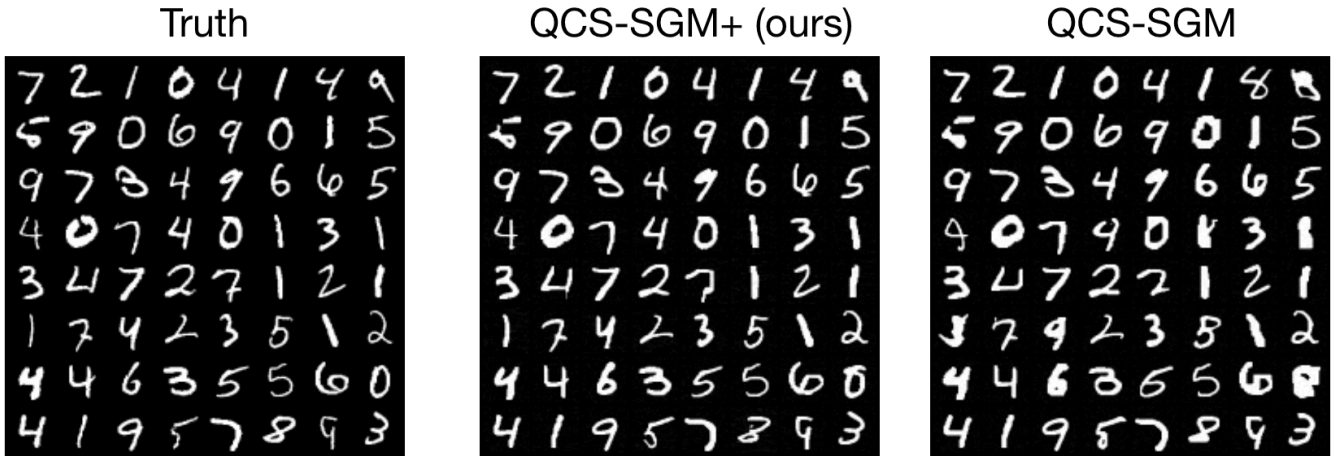
Figure 8: Quantitative comparisons (in terms of SSIM) of the proposed QCS-SGM+ and the original QCS-SGM under 1-bit CS with different levels of additive Gaussian noise for ill-conditioned  $\mathbf{A}$  with condition number  $\kappa = 10^3$ . The number of measurements are set to be  $M = 400, 2000, 4000$  for MNIST, CIFAR-10, and CelebA, respectively, all satisfying  $M < N$ . In all cases, QCS-SGM+ apparently outperforms QCS-SGM.

## B.2 Additional Qualitative Results

In this section, we provide additional qualitative results in various settings, as shown in Figures 9 - 17. The results in Figures 9 - 17 empirically demonstrate that our proposed QCS-SGM+ remarkably outperforms the original QCS-SGM for general matrices beyond mere row-orthogonality.



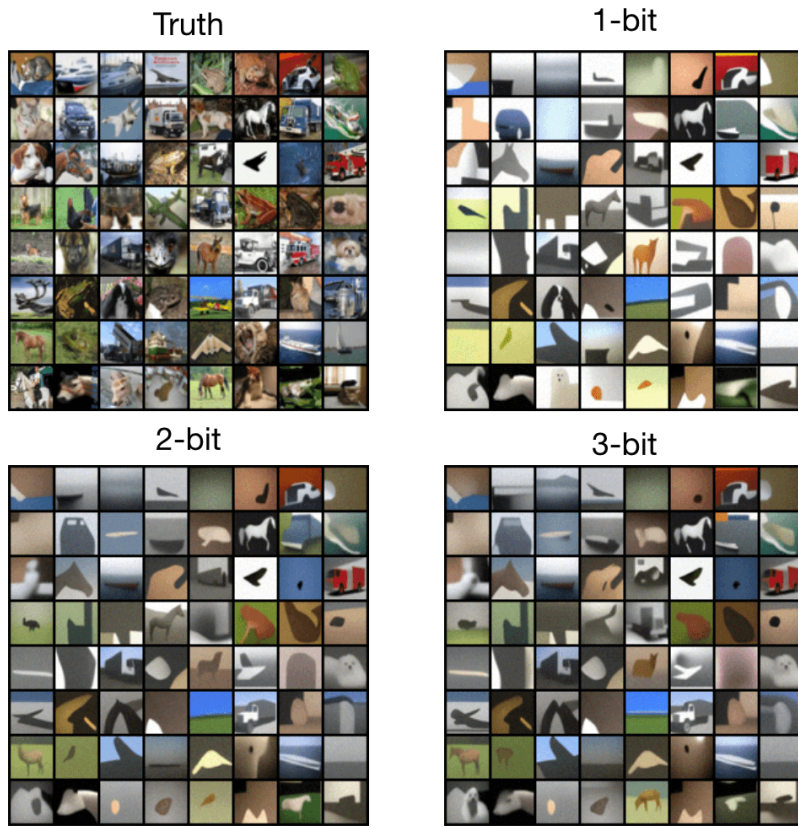
(a) 1-bit CS with ill-conditioned  $\mathbf{A}$ ,  $\kappa = 10^3$ ,  $M = 400$ ,  $\sigma = 0.1$



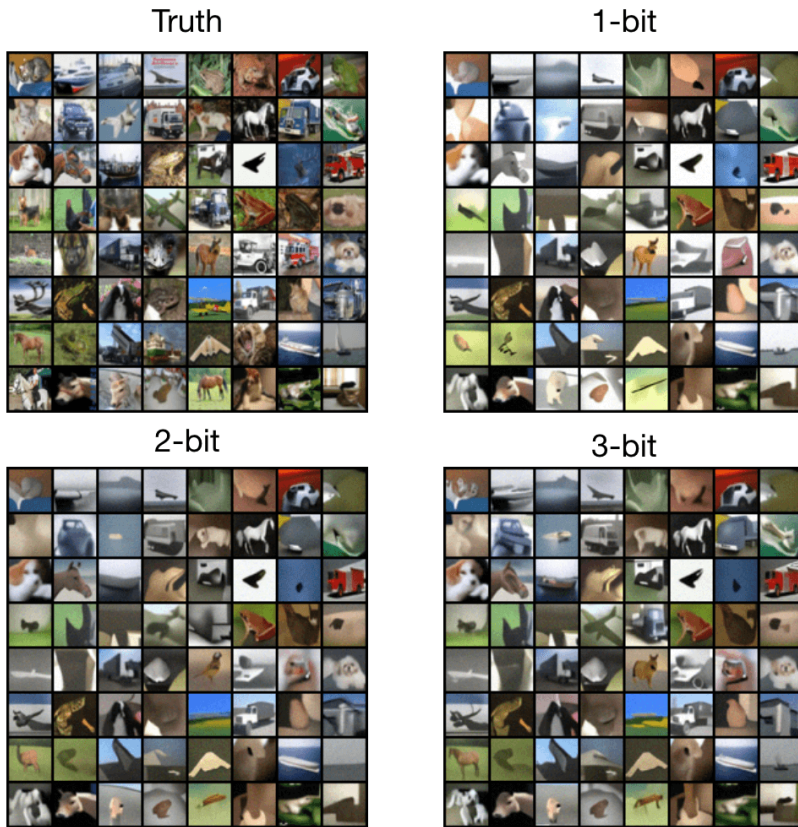
(b) 1-bit CS with correlated  $\mathbf{A}$ ,  $\rho = 0.4$ ,  $M = 400$ ,  $\sigma = 0.1$

Figure 9: Comparison of QCS-SGM and QCS-SGM+ (ours) for 1-bit CS on MNIST with (a) ill-conditioned  $\mathbf{A}$  and (b) correlated  $\mathbf{A}$ , respectively. It can be seen that in both cases QCS-SGM+ outperforms QCS-SGM remarkably.



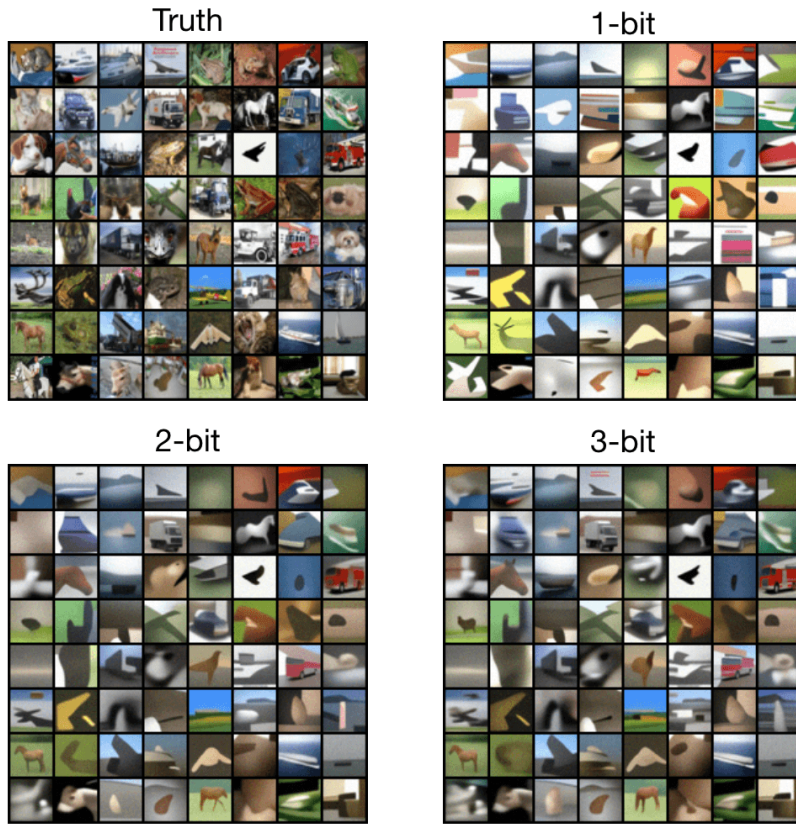


(a) QCS-SGM

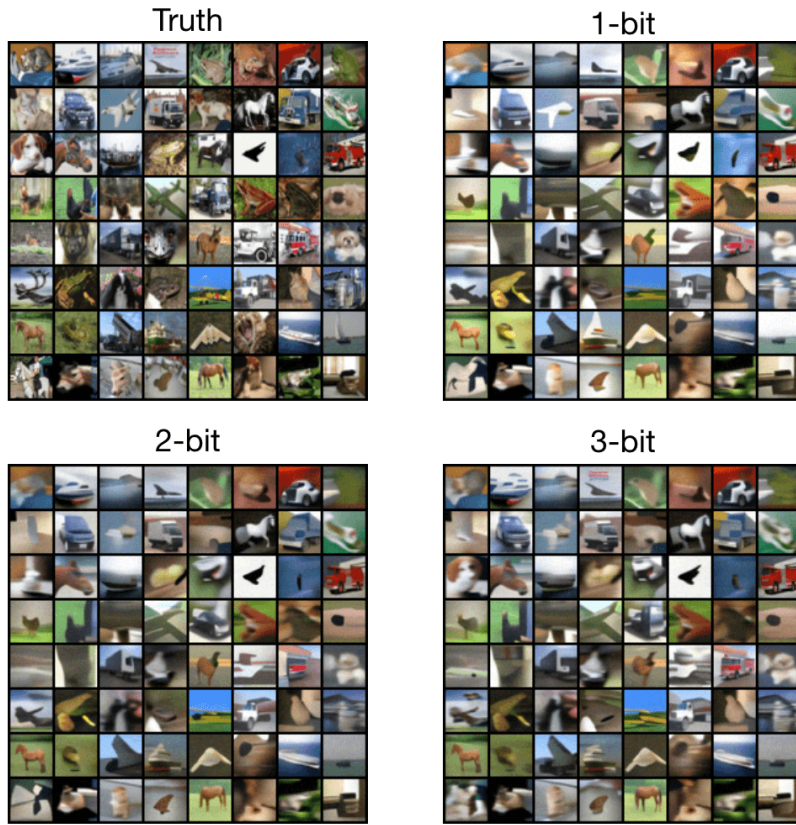


(b) QCS-SGM+ (ours)

Figure 10: Results of QCS-SGM+ and QCS-SGM under 1-3 bit CS on CIFAR-10 for ill-conditioned  $\mathbf{A}$  ( $\kappa = 10^3$ ) when  $M = 2000, \sigma = 0.1$ . QCS-SGM+ outperforms QCS-SGM remarkably.



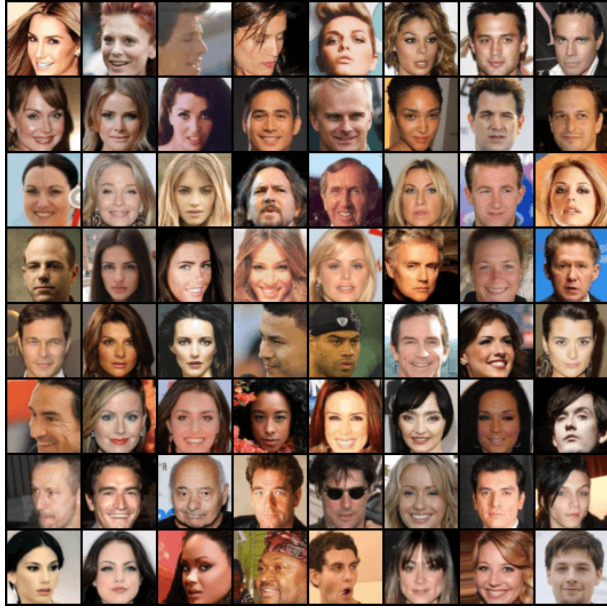
(a) QCS-SGM



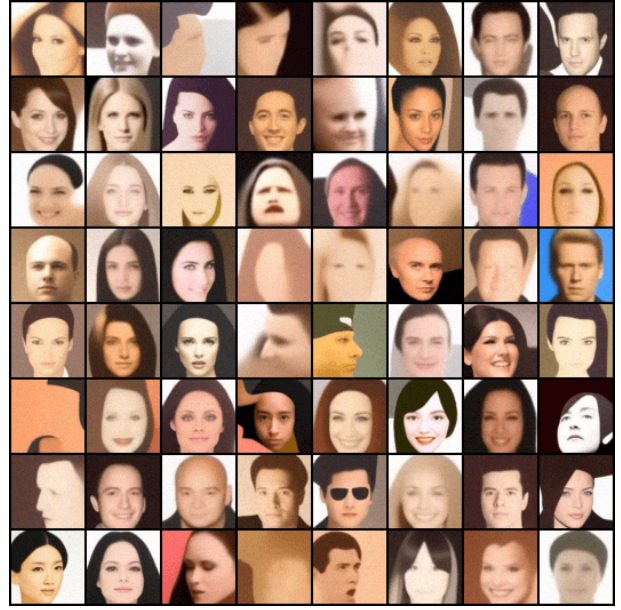
(b) QCS-SGM+ (ours)

Figure 11: Results of QCS-SGM+ and QCS-SGM under 1-3 bit CS on CIFAR-10 for correlated  $\mathbf{A}$  ( $\rho = 0.4$ ) when  $M = 2000, \sigma = 0.1$ . QCS-SGM+ outperforms QCS-SGM remarkably.

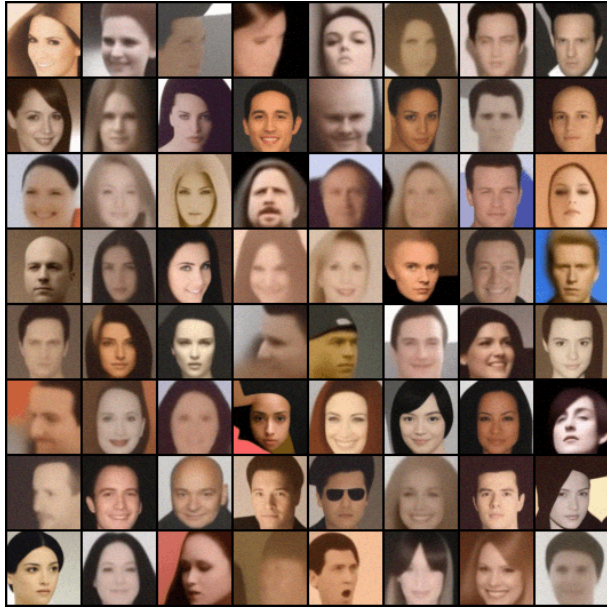




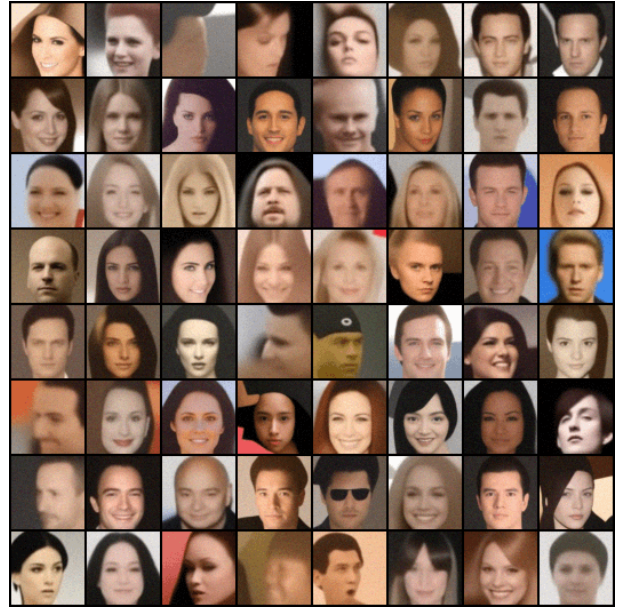
(a) Truth



(b) 1-bit



(c) 2-bit



(d) 3-bit

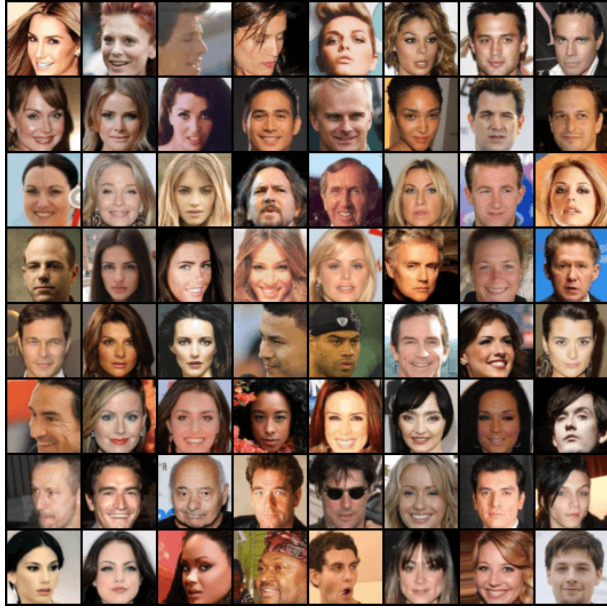
Figure 12: Results of QCS-SGM under 1-3 bit CS on CelebA for ill-conditioned  $\mathbf{A}$  ( $\kappa = 10^3$ ) when  $M = 4000$ ,  $\sigma = 0.1$ .



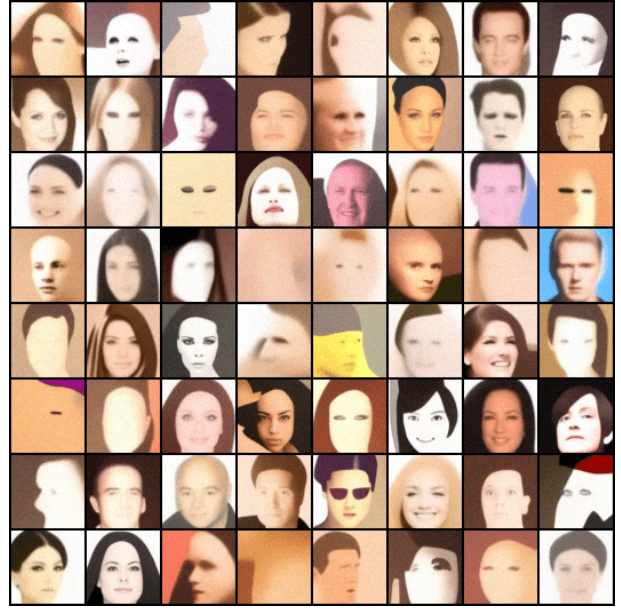


Figure 13: Results of QCS-SGM+ (ours) under 1-3 bit CS on CelebA for ill-conditioned  $\mathbf{A}$  ( $\kappa = 10^3$ ) when  $M = 4000$ ,  $\sigma = 0.1$ . It can be seen that QCS-SGM+ outperforms QCS-SGM in Figure 12 remarkably.

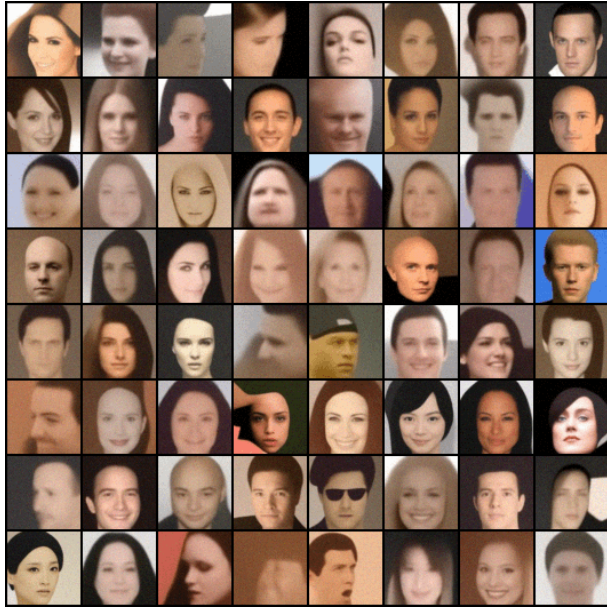




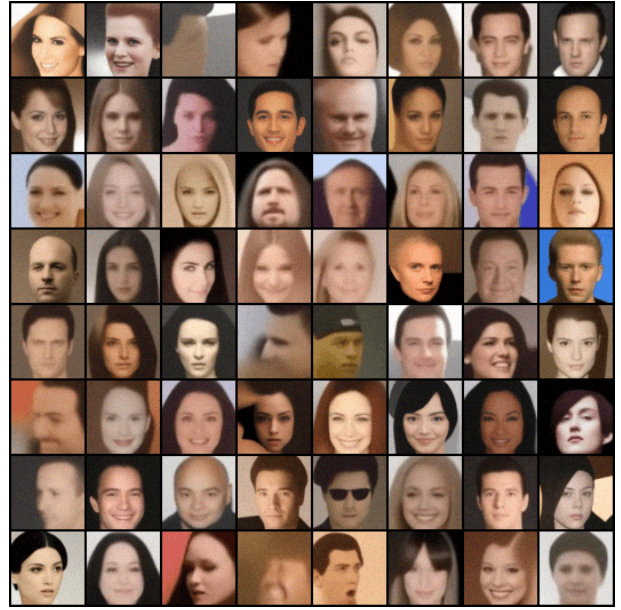
(a) Truth



(b) 1-bit



(c) 2-bit



(d) 3-bit

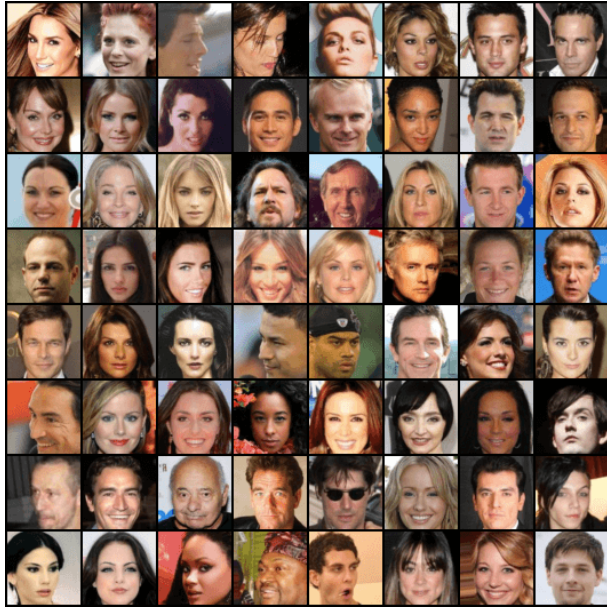
Figure 14: Results of QCS-SGM under 1-3 bit CS on CelebA for ill-conditioned  $\mathbf{A}$  ( $\kappa = 10^6$ ) when  $M = 4000$ ,  $\sigma = 0.1$ .



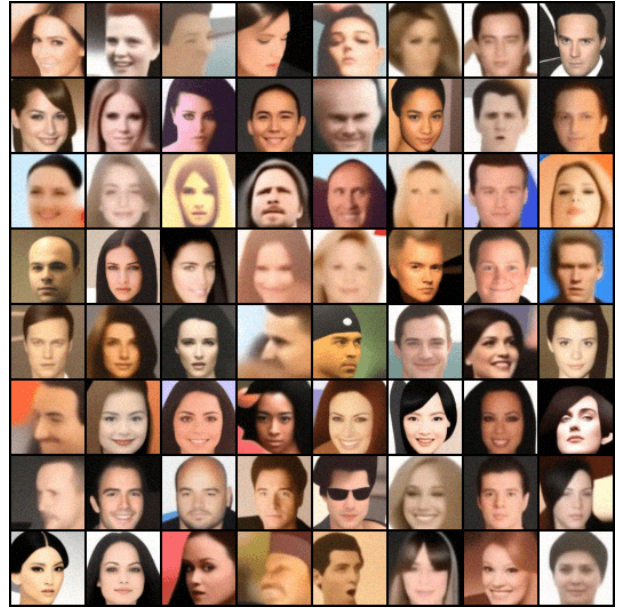


Figure 15: Results of QCS-SGM+ (ours) under 1-3 bit CS on CelebA for ill-conditioned  $\mathbf{A}$  ( $\kappa = 10^3$ ) when  $M = 4000$ ,  $\sigma = 0.1$ . It can be seen that QCS-SGM+ outperforms QCS-SGM in Figure 14 remarkably.

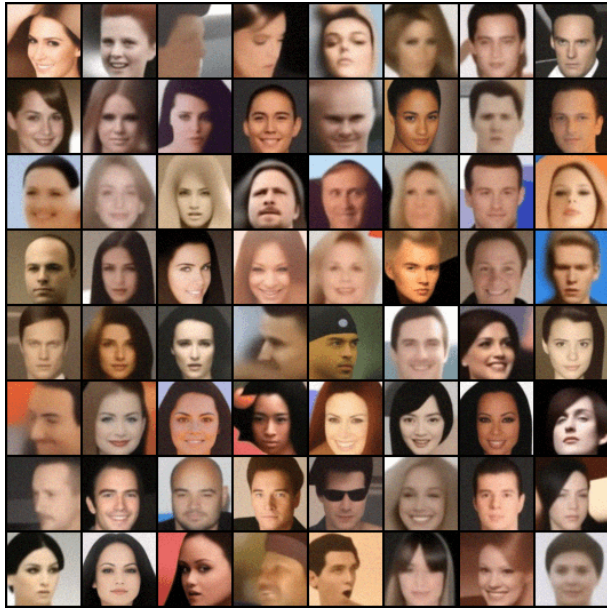




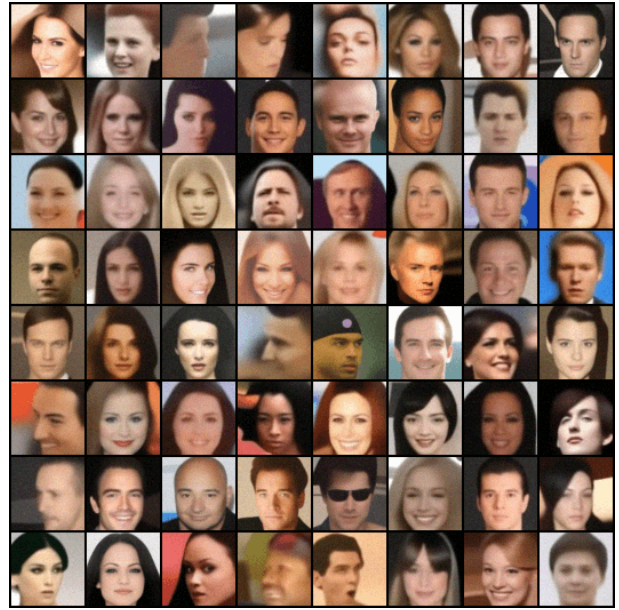
(a) Truth



(b) 1-bit



(c) 2-bit



(d) 3-bit

Figure 16: Results of QCS-SGM under 1-3 bit CS on CelebA for correlated  $\mathbf{A}$  ( $\rho = 0.4$ ) when  $M = 4000, \sigma = 0.1$ .





Figure 17: Results of QCS-SGM+ (ours) under 1-3 bit CS on CelebA for correlated  $\mathbf{A}$  ( $\rho = 0.4$ ) when  $M = 4000$ ,  $\sigma = 0.1$ . It can be seen that QCS-SGM+ outperforms QCS-SGM in Figure 16 remarkably.